EUROPEAN ORGANIZATION FOR NUCLEAR RESEARCH

CERN-PPE/97-28
11 March 1997

Production of Single W Bosons at LEP

L3 Collaboration

Abstract

We report on the observation of single W boson production in a data sample collected by the L3 detector at LEP2. The signal consists of large missing energy final states with a single energetic lepton or two hadronic jets. The cross-section is measured to be $0.61^{+0.43}_{-0.33} \pm 0.05$ pb at the centre of mass energy $\sqrt{s} = 172$ GeV, consistent with the Standard Model expectation. From this measurement the following limits on the anomalous γWW gauge couplings are derived at 95% CL: $-3.6 < \Delta\kappa_\gamma < 1.5$ and $-3.6 < \lambda_\gamma < 3.6$.

Submitted to *Phys.Lett. B*

1 Introduction

The Standard Model of electroweak interactions [1] is successful in describing gauge boson couplings to fermions. Extensive studies of Zff couplings have been performed at LEP in the vicinity of the Z pole [2]. The increase of the LEP energy above the W^+W^- production threshold makes it possible to examine triple gauge boson couplings [3]. Limits on the anomalous couplings have been already reported by the experiments at the Tevatron [4,5] and at LEP [6,7].

Studies of anomalous couplings at LEP have so far focused on the process $e^+e^- \to W^+W^-$, where it is difficult to disentangle the effects of ZWW and γWW couplings. A measurement of the single W production [8] [1)]

$$e^+e^- \to e^+\nu_e W^- \tag{1}$$

constitutes a clean test of the γWW vertex [9]. This process is dominated by contributions from the three diagrams shown in Figure 1.

The deviation of the gauge boson couplings from their Standard Model values is usually described in terms of five parameters: Δg_1^Z, $\Delta\kappa_Z$, $\Delta\kappa_\gamma$, λ_Z and λ_γ. The cross-section of process (1) is shown in reference [8] to depend only on the $\Delta\kappa_\gamma$ and λ_γ parameters.

A specific feature of this reaction is a final state positron (electron) produced at very low polar angle and therefore not detected. Thus the signature of this process is large transverse missing energy and either a single energetic lepton, if the W boson decays into lepton and neutrino, or two hadronic jets in case of hadronic W decays. This process constitutes a background to missing energy searches for new physics beyond the Standard Model. No measurement of single W production has so far been reported at LEP.

In this paper we present a measurement of the cross section for the process $e^+e^- \to e^+\nu_e W^-$ using both leptonic and hadronic decays of W bosons. From this observation we derive limits on the anomalous γWW couplings.

2 Data and Monte Carlo Samples

The data were collected by the L3 detector at LEP in 1996. The integrated luminosities are 10.9 pb^{-1} at the centre of mass energy $\sqrt{s} = 161$ GeV and 10.2 pb^{-1} at $\sqrt{s} = 172$ GeV.

The L3 detector is described in reference [10]. Briefly, the e^+e^- collision point is surrounded by a precision silicon vertex detector, a time-expansion tracking chamber (TEC), a high resolution electromagnetic calorimeter (ECAL), a cylindrical shell of scintillation counters, a hadron calorimeter (HCAL), a muon spectrometer and a very forward calorimeter used for the luminosity measurements. The detector is installed in a large solenoidal magnet providing a 0.5 T field.

For the efficiency studies a sample of $e^+e^- \to e^+\nu_e f\bar{f}'$ events was generated using the GRC4F [11] Monte Carlo generator. For the background studies the following Monte Carlo programs were used: KORALZ [12] ($e^+e^- \to \mu^+\mu^-(\gamma)$, $\tau^+\tau^-(\gamma)$), KORALW [13] ($e^+e^- \to W^+W^- \to f\bar{f}'f\bar{f}'$), BHAGENE3 [14] ($e^+e^- \to e^+e^-(\gamma)$), TEEGG [15] ($e^+e^- \to e^+e^-\gamma$), PYTHIA [16] ($e^+e^- \to q\bar{q}(\gamma)$), PYTHIA and PHOJET [17] ($e^+e^- \to e^+e^-e^+e^-$, $e^+e^-\mu^+\mu^-$, $e^+e^-\tau^+\tau^-$, $e^+e^-q\bar{q}$), and EXCALIBUR [18] ($e^+e^- \to f\bar{f}'f\bar{f}'$).

The Monte Carlo events are simulated in the L3 detector using the GEANT 3.15 program [19], which takes into account the effects of energy loss, multiple scattering and showering in

[1)] The charge conjugate reactions are understood to be included throughout the paper.

the detector. The GHEISHA program [20] is used to simulate hadronic interactions in the detector.

3 Analysis

In the analysis described below, the signal is defined as $e^+e^- \to e^+\nu_e f\bar{f}'$ events that satisfy the following phase space requirements:

$$\begin{aligned} |\cos\theta_{e^+}| &> 0.997 \\ \min(E_f, E_{\bar{f}'}) &> 15 \text{ GeV} \\ |\cos\theta_{e^-}| &< 0.75, \quad \text{for } e^+\nu_e e^-\bar{\nu}_e \text{ events only} \end{aligned} \tag{2}$$

where θ_{e^+} (θ_{e^-}) is the polar angle of the outgoing positron (electron), and E_f and $E_{\bar{f}'}$ are the fermion energies. The final states $e^+e^- \to e^+\nu_e f\bar{f}'$ that do not satisfy these conditions are considered as a background; they consist mostly of the reaction $e^+e^- \to W^+W^-$.

Inside the region of phase space (2) the single W production (process 1) dominates since it peaks strongly at $|\cos\theta_{e^+}| \sim 1$. On average it accounts for 90% of all events in this region, the remaining 10% being mostly non-resonant final states. The purity depends slightly on the flavour of the $f\bar{f}'$ pair from W^- decays.

The above is illustrated in Figure 2 using a Monte Carlo sample of $e^+e^- \to e^+\nu_e\mu^-\bar{\nu}_\mu$ final states. The cosine of the polar angle distribution, $\cos\theta_{e^+}$, is shown in Figure 2a. The invariant mass distributions $M_{\mu^-\bar{\nu}_\mu}$ and $M_{e^+\nu_e}$ for events satisfying phase space conditions (2) are presented in Figures 2b and 2c. Only the $M_{\mu^-\bar{\nu}_\mu}$ spectrum shows resonant behaviour at the W mass; the $M_{e^+\nu_e}$ spectrum is clearly non-resonant since the positron does not originate from a W.

Due to the small data samples at the two centre of mass energies, the data are combined and the cross-section is quoted at $\sqrt{s} = 172$ GeV. The cross-section increases by a factor 1.20 from $\sqrt{s} = 161$ GeV to $\sqrt{s} = 172$ GeV according to the GRC4F predictions. The relative contribution of each final state to the signal is given by the corresponding cross-section and experimental selection efficiency. The selection efficiencies depend slightly on the amount of non-resonant contribution and thus on the anomalous couplings $\Delta\kappa_\gamma$ and λ_γ. In the following measurement this dependence is neglected. This leads to an additional systematic uncertainty which is estimated to be smaller than 5% of the measured cross-section.

3.1 Leptonic Final States

A distinct feature of the process $e^+e^- \to e^+\nu_e W^-$, $W^- \to \ell^-\bar{\nu}_\ell$ is a high energy lepton from W decay with no other significant activity in the detector.

Events with one charged lepton (electron, muon or tau) with an energy of at least 15 GeV are selected. The lepton identification is based on the energy distribution in the electromagnetic and hadron calorimeters with respect to the trajectory of charged tracks. Events containing tracks that do not belong to the lepton are rejected. The visible energy, E_{vis}, is calculated as the sum of the lepton energy, E_ℓ, and the energies of all neutral clusters in the event. The ratio E_ℓ/E_{vis} for events preselected as described above is shown in Figure 3a. The requirement $E_\ell/E_{vis} > 0.9$ suppresses background from two fermion production $e^+e^- \to \ell^+\ell^-(\gamma)$. In addition, the energy in the 0.44 rad azimuthal angle sector along the missing energy direction must be below 1 GeV. For the single electron final states, the polar angle is required to be $|\cos\theta_e| < 0.72$. This requirement

reduces the contribution from Bhabha scattering and from the process $e^+e^- \to e^+e^-\nu\bar{\nu}$ where the e^+e^- pair originates from a low-mass virtual photon.

A high energy lepton from the two fermion processes $e^+e^- \to \ell^+\ell^-(\gamma)$ which matches the above selection criteria is usually produced along with a high energy electron or photon detected in the forward-backward luminosity calorimeters. This correlation is a direct consequence of momentum conservation in the transverse plane. Therefore it is required that the energy deposition in the forward calorimeters, E_{FB}, does not exceed 15 GeV (Figure 3b). Two events satisfy all selection criteria: a 40.5 GeV electron candidate from the $\sqrt{s} = 161$ GeV data sample (shown in Figure 4) and a 28.5 GeV tau candidate from the $\sqrt{s} = 172$ GeV data sample.

The final lepton energy spectrum for the selected events is presented in Figure 5 together with the Monte Carlo expectations for the signal and background. The signal selection efficiencies at $\sqrt{s} = 161$ GeV are found to be (80±4)%, (55±2)% and (30±2)% for $W^- \to e^-\bar{\nu}_e$, $W^- \to \mu^-\bar{\nu}_\mu$ and $W^- \to \tau^-\bar{\nu}_\tau$ decays respectively. Each efficiency decrease slightly at $\sqrt{s} = 172$ GeV by approximately 4% absolute. The background in the $\sqrt{s} = 161$ GeV data sample is estimated to be 0.23 ± 0.08 events of which 0.11 ± 0.01 are from $e^+e^- \to \mu^+\mu^-(\gamma)$ and $e^+e^- \to \tau^+\tau^-(\gamma)$ events, 0.07 ± 0.07 are from $e^+e^- \to e^+e^-(\gamma)$ scattering and 0.05 ± 0.03 are from four-fermion processes. The background from two-photon interactions is found to be negligible. For the $\sqrt{s} = 172$ GeV data sample the background contamination is calculated to be 0.26 ± 0.07 events. The total error on the background is mostly due to the large uncertainty in the number of expected $e^+e^- \to e^+e^-(\gamma)$ events.

3.2 Hadronic Final States

The selection of candidates for the process $e^+e^- \to e^+\nu_e W^-$, $W^- \to q\bar{q}'$ is based on the following requirements: two acoplanar hadronic jets, no leptons, and large missing transverse energy.

High multiplicity hadronic events with more than four charged tracks are selected with large energy deposition in the electromagnetic calorimeter ($E_{ECAL} > 15$ GeV). All energy clusters in the event are combined to form two hadronic jets using the DURHAM algorithm [21]. The energy in the forward luminosity calorimeters is required to be smaller than 50 GeV. These cuts reduce contributions from the pure leptonic final states $e^+e^- \to e^+e^-(\gamma)$, $\mu^+\mu^-(\gamma)$, $\tau^+\tau^-(\gamma)$ and two-photon interactions $e^+e^- \to e^+e^-q\bar{q}$ while keeping a significant fraction of hadronic events from $e^+e^- \to Z(\gamma)$, $e^+e^- \to W^+W^-$ and $e^+e^- \to ZZ$.

To reject events from the two fermion production process $e^+e^- \to q\bar{q}(\gamma)$ the transverse missing energy is required to exceed 10 GeV. The missing momentum vector must be at least 0.30 rad away from the beam axis and the energy in the 0.44 rad sector along its direction must be below 10 GeV. In addition, the opening angle between the two jets in the plane perpendicular to the beam direction must not exceed 3.0 rad and the energy in the 0.70 rad sector along the direction opposite to the two jets must be below 15 GeV.

Events containing identified leptons with energy greater than 15 GeV are rejected in order to suppress the remaining background from $e^+e^- \to W^+W^-$ where one of the W bosons decays into leptons. In addition, three jets are formed for every remaining event using the DURHAM algorithm. The stereo angle defined by the directions of these jets is required to be smaller than 3.0 rad.

Four candidate events are selected in the $\sqrt{s} = 161$ GeV data sample and seven in the $\sqrt{s} = 172$ GeV data sample. A typical candidate event satisfying all selection criteria is shown in Figure 6. The jet-jet invariant mass spectrum of the selected candidates, M_{inv}, is shown in

Figure 7 together with the fitted signal and the Monte Carlo background predictions.

Events with invariant mass smaller than 100 GeV are used for the cross-section determination. This requirement rejects one candidate from the $\sqrt{s} = 172$ GeV data sample and reduces significantly the background contamination. The signal efficiency is then found to be $(41 \pm 2)\%$, independent of the centre of mass energy. The background is estimated to be 2.1 ± 0.1 events for the $\sqrt{s} = 161$ GeV data and 4.1 ± 0.2 events for the $\sqrt{s} = 172$ GeV data sample.

4 Results

The total cross-section of all signal processes is determined from a binned likelihood fit to the distributions presented in Figures 5 and 7. The background shapes and normalisations are fixed to the Monte Carlo prediction. The fitted signal cross-section, $\sigma(\mathrm{e^+e^-} \to \mathrm{e}\nu_\mathrm{e}\mathrm{W})$, corresponds to that of the process $\mathrm{e^+e^-} \to \mathrm{e}\nu_\mathrm{e}\mathrm{f}\bar{\mathrm{f}}'$, where $\mathrm{f}\bar{\mathrm{f}}'$ denotes a sum of $\ell\nu_\ell$ and $\mathrm{q}\bar{\mathrm{q}}'$ final states satisfying the phase space conditions (2). The measured values of the W branching fractions [22] are assumed in the fit. The relative contribution of the non-resonant $\mathrm{e}\nu_\mathrm{e}\mathrm{f}\bar{\mathrm{f}}'$ final states to the signal is fixed to the GRC4F prediction. The total cross-section is found to be

$$\sigma(\mathrm{e^+e^-} \to \mathrm{e}\nu_\mathrm{e}\mathrm{W}) = 0.61^{+0.43}_{-0.33} \pm 0.05 \text{ pb} \tag{3}$$

at $\sqrt{s} = 172$ GeV. The first error represents statistics and the second one accounts for the experimental systematics due to the uncertainties in the efficiency and the background contamination. The measured cross-section value is consistent with the Standard Model prediction of 0.35 pb calculated with GRC4F. This is the first experimental measurement of the process $\mathrm{e^+e^-} \to \mathrm{e^+}\nu_\mathrm{e}\mathrm{W^-}$.

The total cross-section for the leptonic final states (2) is measured to be

$$\sigma(\mathrm{e^+e^-} \to \mathrm{e}\nu_\mathrm{e}\ell\nu_\ell) = 0.17^{+0.20}_{-0.12} \pm 0.02 \text{ pb}$$

at $\sqrt{s} = 172$ GeV using the same fitting technique. The total cross-section for the hadronic final states (2) is found to be

$$\sigma(\mathrm{e^+e^-} \to \mathrm{e}\nu_\mathrm{e}\mathrm{q}\bar{\mathrm{q}}') = 0.45^{+0.41}_{-0.32} \pm 0.04 \text{ pb}.$$

The signal cross-section as a function of anomalous couplings is calculated with GRC4F. Using the same fitting technique as for the cross-section measurement, the following limits on $\Delta\kappa_\gamma$ and λ_γ are obtained:

$$\begin{aligned} -3.6 \;<\; \lambda_\gamma \;<\; 3.6 \quad &\text{at } 95\% \text{ CL.} \\ -3.6 \;<\; \Delta\kappa_\gamma \;<\; 1.5 \quad &\text{at } 95\% \text{ CL.} \end{aligned} \tag{4}$$

The 63% and 95% contours are presented in Figure 8. These limits are comparable to similar limits on anomalous couplings reported at the Tevatron [4, 5].

Acknowledgements

We wish to express our gratitude to the CERN accelerator divisions for the good performance of the LEP machine. We acknowledge the efforts of all engineers and technicians who have participated in the construction and maintenance of this experiment.

References

[1] S.L.Glashow, Nucl.Phys. **22** (1961) 579;
S.Weinberg, Phys.Rev.Lett. **19** (1967) 1264;
A.Salam, "Elementary Particle Theory", Ed. N. Svartholm, Stockholm, "Almquist and Wiksell", (1968), 367.

[2] D.Buskulic *et al.*, ALEPH Collaboration, Z.Phys. **C62** (1994) 539; P.Abreu *et al.*, DELPHI Collaboration, Nucl.Phys. **B418** (1994) 403; M.Acciarri *et al.*, L3 Collaboration, Z.Phys. **C62** (1994) 551; R.Akers *et al.*, OPAL Collaboration, Z.Phys. **C61** (1994) 19.

[3] Physics at LEP2, edited by G.Altarelli, T.Sjostrand and F.Zwirner, CERN 96-01 (1996).

[4] F.Abe *et al.*, CDF Collaboration, Phys.Rev.Lett. **74** (1995) 1936; F.Abe *et al.*, CDF Collaboration, Phys.Rev.Lett. **75** (1995) 1017; F.Abe *et al.*, CDF Collaboration, FERMILAB Pub-96/311-E, September 1996.

[5] S.Abachi *et al.*, D0 Collaboration, Phys.Rev.Lett. **75** (1995) 1034; S.Abachi *et al.*, D0 Collaboration, FERMILAB-Pub-96/434-E, December 1996.

[6] M.Acciarri *et al.*, L3 Collaboration, CERN-PPE/97-014, to be published in Phys. Lett. **B**.

[7] K.Ackerstaff *et al.*, OPAL Collaboration, CERN-PPE/97-04, to be published in Phys.Lett. **B**; P.Abreu *et al.*, DELPHI Collaboration, CERN-PPE/97-07, to be published in Phys.Lett. **B**.

[8] T.Tsukamoto and Y.Kurihara, Phys.Lett. **B389** (1996), 162.

[9] C.G.Papadopoulos, Phys.Lett. **B333** (1994) 202.

[10] L3 Collaboration, B.Adeva *et al.*, Nucl.Instr.Meth. **A289** (1990) 35; J.A.Bakken *et al.*, Nucl.Instr.Meth. **A275** (1989) 81; O.Adriani *et al.*, Nucl.Instr.Meth. **A302** (1991) 53; B. Adeva *et al.*, Nucl.Instr.Meth. **A323** (1992) 109; K.Deiters *et al.*, Nucl.Instr.Meth. **A323** (1992) 162; B.Acciari *et al.*, Nucl.Instr.Meth. **A351** (1994) 300; A. Adam *et al.*, Nucl.Instr.Meth. **A383** (1996) 342.

[11] J.Fujimoto *et al.*, KEK-CP-046, hep-ph/9603394, to be published in Comp. Phys. Comm.

[12] S.Jadach, B.F.L.Ward and Z.Was, Comp.Phys.Comm. **79** (1994) 503.

[13] M.Skrzypek *et al.*, Comp.Phys.Comm. **94** (1996) 216; M.Skrzypek *et al.*, Phys.Lett. **B372** (1996) 289.

[14] J.H.Field, Phys.Lett. **B323** (1994) 432; J.H.Field and T. Riemann, Comp.Phys.Comm. **94** (1996) 53.

[15] D.Karlen, Nucl.Phys. **B289** (1987) 23.

[16] T.Sjöstrand, CERN-TH/7112/93 (1993), revised August 1995; T.Sjöstrand, Comp. Phys. Comm. 82 (1994) 74.

[17] R.Engel, Z.Phys. **C66** (1995) 203; R.Engel, J.Ranft and S.Roesler, Phys.Rev. **D52** (1995) 1459.

[18] F.A.Berends, R.Kleiss and R.Pittau, Nucl. Phys. **B 424** (1994) 308; Nucl. Phys. **B 426** (1994) 344; Nucl. Phys. (Proc. Suppl.) **B 37** (1994) 163; Phys. Lett. **B 335** (1994) 490; R.Kleiss and R.Pittau, Comp. Phys. Comm. **83** (1994) 14.

[19] R.Brun *et al.*, preprint CERN DD/EE/84-1 (Revised 1987).

[20] H.Fesefeldt, RWTH Aachen Report PITHA 85/02 (1985).

[21] S.Catani *et al.*, Phys. Lett. **B 263** (1991) 491;
S.Bethke *et al.*, Nucl. Phys. **B 370** (1992) 310.

[22] R.M.Barnett *et al.*, Particle Data Group Phys.Rev. **D54** (1996) 1.

The L3 Collaboration:

M.Acciarri,[29] O.Adriani,[18] M.Aguilar-Benitez,[28] S.Ahlen,[12] B.Alpat,[36] J.Alcaraz,[28] G.Alemanni,[24] J.Allaby,[19] A.Aloisio,[31] G.Alverson,[13] M.G.Alviggi,[31] G.Ambrosi,[21] H.Anderhub,[51] V.P.Andreev,[7,40] T.Angelescu,[14] F.Anselmo,[10] A.Arefiev,[30] T.Azemoon,[3] T.Aziz,[11] P.Bagnaia,[39] L.Baksay,[46] S.Banerjee,[11] K.Banicz,[48] R.Barillère,[19] L.Barone,[39] P.Bartalini,[36] A.Baschirotto,[29] M.Basile,[10] R.Battiston,[36] A.Bay,[24] F.Becattini,[18] U.Becker,[17] F.Behner,[51] J.Berdugo,[28] P.Berges,[17] B.Bertucci,[19] B.L.Betev,[51] S.Bhattacharya,[11] M.Biasini,[19] A.Biland,[51] G.M.Bilei[36] J.J.Blaising,[4] S.C.Blyth,[37] G.J.Bobbink,[2] R.Bock,[1] A.Böhm,[1] B.Borgia,[39] D.Bourilkov,[51] M.Bourquin,[21] S.Braccini,[21] J.G.Branson,[42] V.Brigljevic,[51] I.C.Brock,[37] A.Buffini,[18] A.Buijs,[47] J.D.Burger,[17] W.J.Burger,[21] J.Busenitz,[46] A.Button,[3] X.D.Cai,[17] M.Campanelli,[51] M.Capell,[17] G.Cara Romeo,[10] M.Caria,[36] G.Carlino,[31] A.M.Cartacci,[18] J.Casaus,[28] G.Castellini,[18] F.Cavallari,[39] N.Cavallo,[31] C.Cecchi,[21] M.Cerrada,[28] F.Cesaroni,[25] M.Chamizo,[28] A.Chan,[53] Y.H.Chang,[53] U.K.Chaturvedi,[20] S.V.Chekanov,[33] M.Chemarin,[27] A.Chen,[53] G.Chen,[8] G.M.Chen,[8] H.F.Chen,[22] H.S.Chen,[8] X.Chereau,[4] G.Chiefari,[31] C.Y.Chien,[5] L.Cifarelli,[41] F.Cindolo,[10] C.Civinini,[18] I.Clare,[17] R.Clare,[17] H.O.Cohn,[34] G.Coignet,[4] A.P.Colijn,[2] N.Colino,[28] V.Commichau,[1] S.Costantini,[33] F.Cotorobai,[14] B.de la Cruz,[28] A.Csilling,[15] T.S.Dai,[17] R.D'Alessandro,[18] R.de Asmundis,[31] A.Degré,[4] K.Deiters,[49] D.della Volpe,[31] P.Denes,[38] F.DeNotaristefani,[39] D.DiBitonto,[46] M.Diemoz,[39] D.van Dierendonck,[2] F.Di Lodovico,[51] C.Dionisi,[39] M.Dittmar,[51] A.Dominguez,[42] A.Doria,[31] M.T.Dova,[20,♯] E.Drago,[31] D.Duchesneau,[4] P.Duinker,[2] I.Duran,[43] S.Dutta,[11] S.Easo,[36] Yu.Efremenko,[34] H.El Mamouni,[27] A.Engler,[37] F.J.Eppling,[17] F.C.Erné,[2] J.P.Ernenwein,[27] P.Extermann,[21] M.Fabre,[49] R.Faccini,[39] S.Falciano,[39] A.Favara,[18] J.Fay,[27] O.Fedin,[40] M.Felcini,[51] B.Fenyi,[46] T.Ferguson,[37] F.Ferroni,[39] H.Fesefeldt,[1] E.Fiandrini,[36] J.H.Field,[21] F.Filthaut,[37] P.H.Fisher,[17] G.Forconi,[17] L.Fredj,[21] K.Freudenreich,[51] C.Furetta,[29] Yu.Galaktionov,[30,17] S.N.Ganguli,[11] P.Garcia-Abia,[50] S.S.Gau,[13] S.Gentile,[39] N.Gheordanescu,[14] S.Giagu,[39] S.Goldfarb,[24] J.Goldstein,[12] Z.F.Gong,[22] A.Gougas,[5] G.Gratta,[35] M.W.Gruenewald,[9] V.K.Gupta,[38] A.Gurtu,[11] L.J.Gutay,[48] B.Hartmann,[1] A.Hasan,[32] D.Hatzifotiadou,[10] T.Hebbeker,[9] A.Hervé,[19] W.C.van Hoek,[33] H.Hofer,[51] S.J.Hong,[45] H.Hoorani,[37] S.R.Hou,[53] G.Hu,[5] V.Innocente,[19] K.Jenkes,[1] B.N.Jin,[8] L.W.Jones,[3] P.de Jong,[19] I.Josa-Mutuberria,[28] A.Kasser,[24] R.A.Khan,[20] D.Kamrad,[50] Yu.Kamyshkov,[34] J.S.Kapustinsky,[26] Y.Karyotakis,[4] M.Kaur,[20,◇] M.N.Kienzle-Focacci,[21] D.Kim,[5] D.H.Kim,[45] J.K.Kim,[45] S.C.Kim,[45] Y.G.Kim,[45] W.W.Kinnison,[26] A.Kirkby,[35] D.Kirkby,[35] J.Kirkby,[19] D.Kiss,[15] W.Kittel,[33] A.Klimentov,[17,30] A.C.König,[33] I.Korolko,[30] V.Koutsenko,[17,30] R.W.Kraemer,[37] W.Krenz,[1] A.Kunin,[17,30] P.Ladron de Guevara,[28] I.Laktineh,[27] G.Landi,[18] C.Lapoint,[17] K.Lassila-Perini,[51] P.Laurikainen,[23] M.Lebeau,[19] A.Lebedev,[17] P.Lebrun,[27] P.Lecomte,[51] P.Lecoq,[19] P.Le Coultre,[51] J.M.Le Goff,[19] R.Leiste,[50] E.Leonardi,[39] P.Levtchenko,[40] C.Li,[22] E.Lieb,[50] W.T.Lin,[53] F.L.Linde,[2,19] L.Lista,[31] Z.A.Liu,[8] W.Lohmann,[50] E.Longo,[39] W.Lu,[35] Y.S.Lu,[8] K.Lübelsmeyer,[1] C.Luci,[39] D.Luckey,[17] L.Luminari,[39] W.Lustermann,[49] W.G.Ma,[22] M.Maity,[11] G.Majumder,[11] L.Malgeri,[39] A.Malinin,[30] C.Maña,[28] D.Mangeol,[33] S.Mangla,[11] P.Marchesini,[51] A.Marin,[12] J.P.Martin,[27] F.Marzano,[39] G.G.G.Massaro,[2] D.McNally,[19] R.R.McNeil,[7] S.Mele,[31] L.Merola,[31] M.Meschini,[18] W.J.Metzger,[33] M.von der Mey,[1] Y.Mi,[24] A.Mihul,[14] A.J.W.van Mil,[33] G.Mirabelli,[39] J.Mnich,[19] P.Molnar,[9] B.Monteleoni,[18] R.Moore,[3] S.Morganti,[39] T.Moulik,[11] R.Mount,[35] S.Müller,[1] F.Muheim,[21] A.J.M.Muijs,[2] E.Nagy,[15] S.Nahn,[17] M.Napolitano,[31] F.Nessi-Tedaldi,[51] H.Newman,[35] T.Niessen,[1] A.Nippe,[1] A.Nisati,[39] H.Nowak,[50] Y.D.Oh,[45] H.Opitz,[1] G.Organtini,[39] R.Ostonen,[23] C.Palomares,[28] D.Pandoulas,[1] S.Paoletti,[39] P.Paolucci,[31] H.K.Park,[37] I.H.Park,[45] G.Pascale,[39] G.Passaleva,[18] S.Patricelli,[31] T.Paul,[13] M.Pauluzzi,[36] C.Paus,[1] F.Pauss,[51] D.Peach,[19] Y.J.Pei,[1] S.Pensotti,[29] D.Perret-Gallix,[4] B.Petersen,[33] S.Petrak,[9] A.Pevsner,[5] D.Piccolo,[31] M.Pieri,[18] J.C.Pinto,[37] P.A.Piroué,[38] E.Pistolesi,[29] V.Plyaskin,[30] M.Pohl,[51] V.Pojidaev,[30,18] H.Postema,[17] N.Produit,[21] D.Prokofiev,[40] G.Rahal-Callot,[51] P.G.Rancoita,[29] M.Rattaggi,[29] G.Raven,[42] P.Razis,[32] K.Read,[34] D.Ren,[51] M.Rescigno,[39] S.Reucroft,[13] T.van Rhee,[47] S.Riemann,[50] K.Riles,[3] A.Robohm,[51] J.Rodin,[17] B.P.Roe,[3] L.Romero,[28] S.Rosier-Lees,[4] Ph.Rosselet,[24] W.van Rossum,[47] S.Roth,[1] J.A.Rubio,[19] D.Ruschmeier,[9] H.Rykaczewski,[51] J.Salicio,[19] E.Sanchez,[28] M.P.Sanders,[33] A.Santocchia,[36] M.E.Sarakinos,[23] S.Sarkar,[11] M.Sassowsky,[1] C.Schäfer,[1] V.Schegelsky,[40] S.Schmidt-Kaerst,[1] D.Schmitz,[1] P.Schmitz,[1] N.Scholz,[51] H.Schopper,[52] D.J.Schotanus,[33] J.Schwenke,[1] G.Schwering,[1] C.Sciacca,[31] D.Sciarrino,[21] L.Servoli,[36] S.Shevchenko,[35] N.Shivarov,[44] V.Shoutko,[30] J.Shukla,[26] E.Shumilov,[30] A.Shvorob,[35] T.Siedenburg,[1] D.Son,[45] A.Sopczak,[50] B.Smith,[17] P.Spillantini,[18] M.Steuer,[17] D.P.Stickland,[38] H.Stone,[38] B.Stoyanov,[44] A.Straessner,[1] K.Strauch,[16] K.Sudhakar,[11] G.Sultanov,[20] L.Z.Sun,[22] G.F.Susinno,[21] H.Suter,[51] J.D.Swain,[20] X.W.Tang,[8] L.Tauscher,[6] L.Taylor,[13] Samuel C.C.Ting,[17] S.M.Ting,[17] M.Tonutti,[1] S.C.Tonwar,[11] J.Tóth,[15] C.Tully,[38] H.Tuchscherer,[46] K.L.Tung,[8] Y.Uchida,[17] J.Ulbricht,[51] U.Uwer,[19] E.Valente,[39] R.T.Van de Walle,[33] G.Vesztergombi,[15] I.Vetlitsky,[30] G.Viertel,[51] M.Vivargent,[4] R.Völkert,[50] H.Vogel,[37] H.Vogt,[50] I.Vorobiev,[30] A.A.Vorobyov,[40] A.Vorvolakos,[32] M.Wadhwa,[6] W.Wallraff,[1] J.C.Wang,[17] X.L.Wang,[22] Z.M.Wang,[22] A.Weber,[1] F.Wittgenstein,[19] S.X.Wu,[20] S.Wynhoff,[1] J.Xu,[12] Z.Z.Xu,[22] B.Z.Yang,[22] C.G.Yang,[8] X.Y.Yao,[8] J.B.Ye,[22] S.C.Yeh,[53] J.M.You,[37] An.Zalite,[40] Yu.Zalite,[40] P.Zemp,[51] Y.Zeng,[1] Z.Zhang,[8] Z.P.Zhang,[22] B.Zhou,[12] G.Y.Zhu,[8] R.Y.Zhu,[35] A.Zichichi,[10,19,20] F.Ziegler.[50]

1 I. Physikalisches Institut, RWTH, D-52056 Aachen, FRG§
III. Physikalisches Institut, RWTH, D-52056 Aachen, FRG§
2 National Institute for High Energy Physics, NIKHEF, and University of Amsterdam, NL-1009 DB Amsterdam, The Netherlands
3 University of Michigan, Ann Arbor, MI 48109, USA
4 Laboratoire d'Annecy-le-Vieux de Physique des Particules, LAPP,IN2P3-CNRS, BP 110, F-74941 Annecy-le-Vieux CEDEX, France
5 Johns Hopkins University, Baltimore, MD 21218, USA
6 Institute of Physics, University of Basel, CH-4056 Basel, Switzerland
7 Louisiana State University, Baton Rouge, LA 70803, USA
8 Institute of High Energy Physics, IHEP, 100039 Beijing, China△
9 Humboldt University, D-10099 Berlin, FRG§
10 University of Bologna and INFN-Sezione di Bologna, I-40126 Bologna, Italy
11 Tata Institute of Fundamental Research, Bombay 400 005, India
12 Boston University, Boston, MA 02215, USA
13 Northeastern University, Boston, MA 02115, USA
14 Institute of Atomic Physics and University of Bucharest, R-76900 Bucharest, Romania
15 Central Research Institute for Physics of the Hungarian Academy of Sciences, H-1525 Budapest 114, Hungary‡
16 Harvard University, Cambridge, MA 02139, USA
17 Massachusetts Institute of Technology, Cambridge, MA 02139, USA
18 INFN Sezione di Firenze and University of Florence, I-50125 Florence, Italy
19 European Laboratory for Particle Physics, CERN, CH-1211 Geneva 23, Switzerland
20 World Laboratory, FBLJA Project, CH-1211 Geneva 23, Switzerland
21 University of Geneva, CH-1211 Geneva 4, Switzerland
22 Chinese University of Science and Technology, USTC, Hefei, Anhui 230 029, China△
23 SEFT, Research Institute for High Energy Physics, P.O. Box 9, SF-00014 Helsinki, Finland
24 University of Lausanne, CH-1015 Lausanne, Switzerland
25 INFN-Sezione di Lecce and Universitá Degli Studi di Lecce, I-73100 Lecce, Italy
26 Los Alamos National Laboratory, Los Alamos, NM 87544, USA
27 Institut de Physique Nucléaire de Lyon, IN2P3-CNRS,Université Claude Bernard, F-69622 Villeurbanne, France
28 Centro de Investigaciones Energeticas, Medioambientales y Tecnologicas, CIEMAT, E-28040 Madrid, Spain♭
29 INFN-Sezione di Milano, I-20133 Milan, Italy
30 Institute of Theoretical and Experimental Physics, ITEP, Moscow, Russia
31 INFN-Sezione di Napoli and University of Naples, I-80125 Naples, Italy
32 Department of Natural Sciences, University of Cyprus, Nicosia, Cyprus
33 University of Nijmegen and NIKHEF, NL-6525 ED Nijmegen, The Netherlands
34 Oak Ridge National Laboratory, Oak Ridge, TN 37831, USA
35 California Institute of Technology, Pasadena, CA 91125, USA
36 INFN-Sezione di Perugia and Universitá Degli Studi di Perugia, I-06100 Perugia, Italy
37 Carnegie Mellon University, Pittsburgh, PA 15213, USA
38 Princeton University, Princeton, NJ 08544, USA
39 INFN-Sezione di Roma and University of Rome, "La Sapienza", I-00185 Rome, Italy
40 Nuclear Physics Institute, St. Petersburg, Russia
41 University and INFN, Salerno, I-84100 Salerno, Italy
42 University of California, San Diego, CA 92093, USA
43 Dept. de Fisica de Particulas Elementales, Univ. de Santiago, E-15706 Santiago de Compostela, Spain
44 Bulgarian Academy of Sciences, Central Lab. of Mechatronics and Instrumentation, BU-1113 Sofia, Bulgaria
45 Center for High Energy Physics, Korea Adv. Inst. of Sciences and Technology, 305-701 Taejon, Republic of Korea
46 University of Alabama, Tuscaloosa, AL 35486, USA
47 Utrecht University and NIKHEF, NL-3584 CB Utrecht, The Netherlands
48 Purdue University, West Lafayette, IN 47907, USA
49 Paul Scherrer Institut, PSI, CH-5232 Villigen, Switzerland
50 DESY-Institut für Hochenergiephysik, D-15738 Zeuthen, FRG
51 Eidgenössische Technische Hochschule, ETH Zürich, CH-8093 Zürich, Switzerland
52 University of Hamburg, D-22761 Hamburg, FRG
53 High Energy Physics Group, Taiwan, China

§ Supported by the German Bundesministerium für Bildung, Wissenschaft, Forschung und Technologie
‡ Supported by the Hungarian OTKA fund under contract number T024011..
♭ Supported also by the Comisión Interministerial de Ciencia y Tecnología
♯ Also supported by CONICET and Universidad Nacional de La Plata, CC 67, 1900 La Plata, Argentina
♢ Also supported by Panjab University, Chandigarh-160014, India
△ Supported by the National Natural Science Foundation of China.

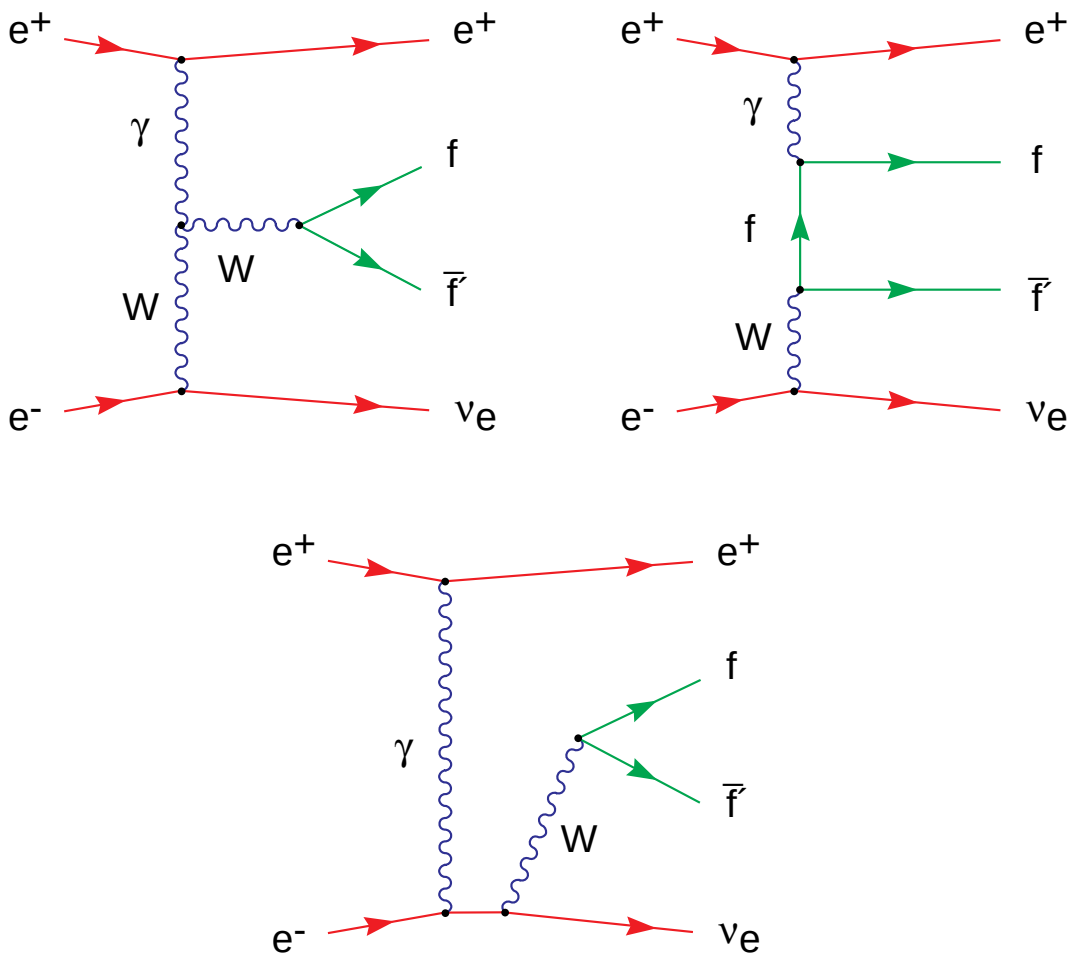

Figure 1: The dominant Feynman diagrams for the process (1).

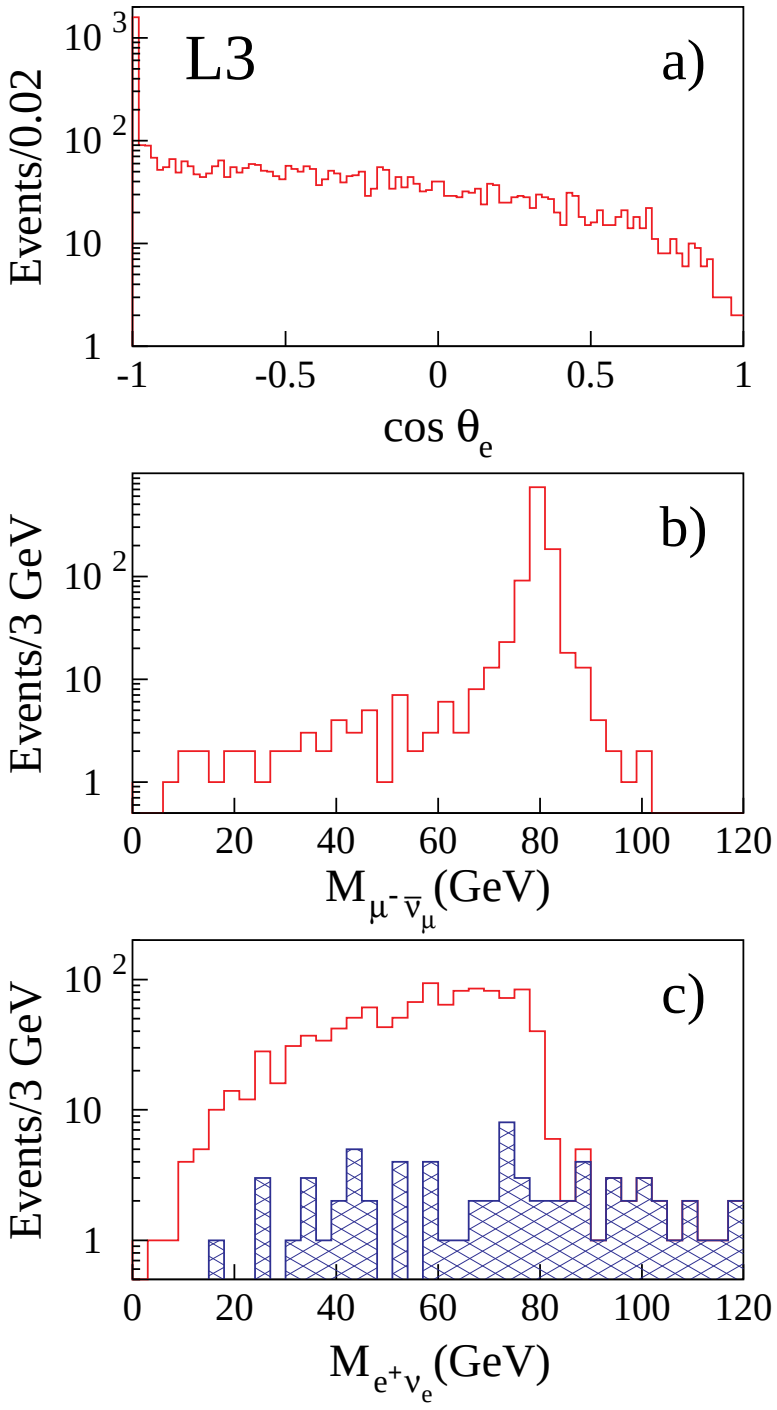

Figure 2: (a) The positron polar angle spectrum for all $e^+\nu_e\mu^-\bar{\nu}_\mu$ final states generated by GRC4F at $\sqrt{s} = 161$ GeV. The invariant mass spectrum of the $\mu^-\bar{\nu}_\mu$ (b) and $e^+\nu_e$ (c) pairs for the events satisfying phase space conditions (2). The hatched histogram in (c) represents events which meet the requirement $|M_{\mu\nu_\mu} - M_W| > 10$ GeV.

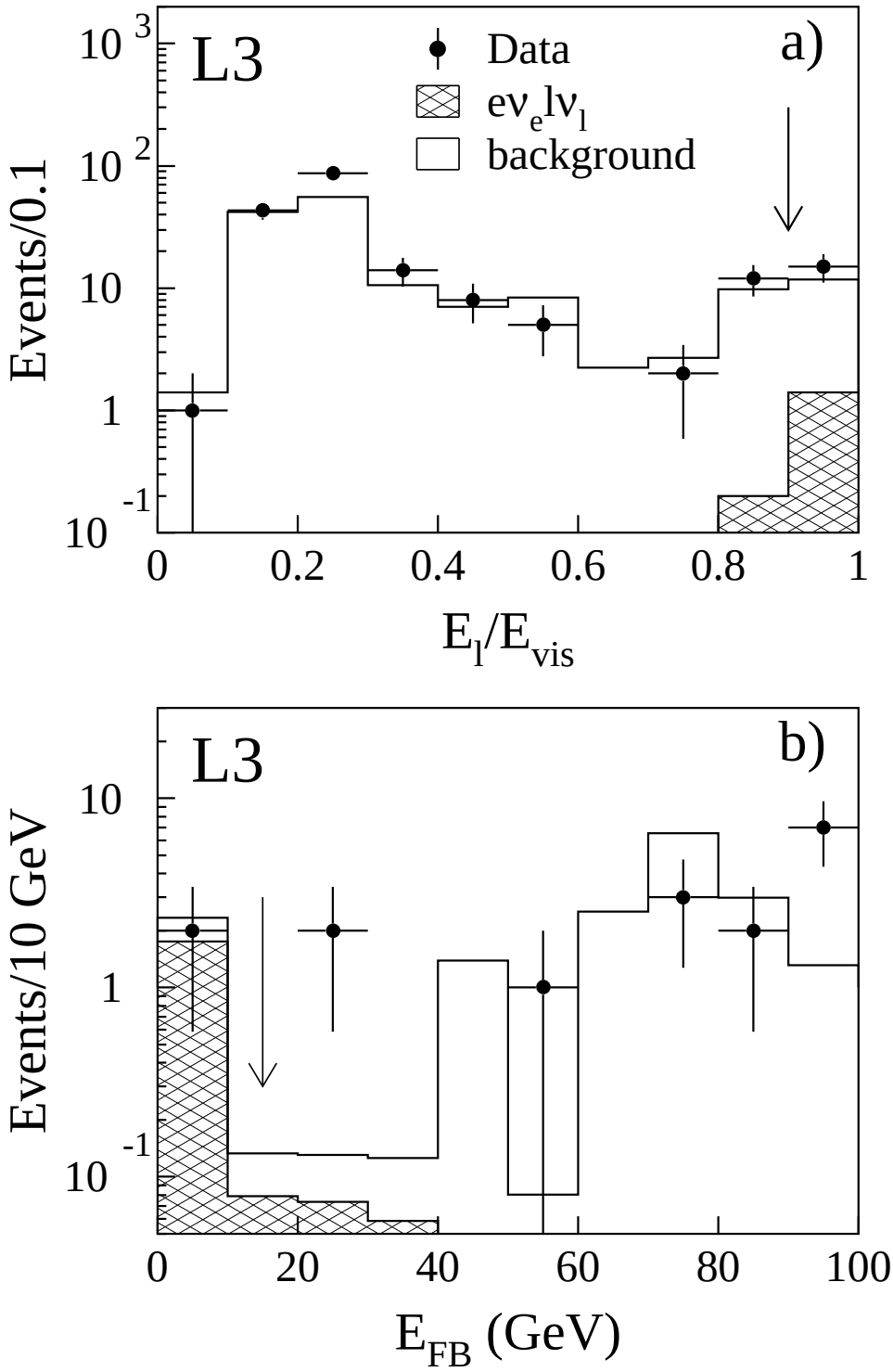

Figure 3: (a) The ratio E_ℓ/E_{vis} for the preselected single lepton data sample. (b) The spectrum of energy depositions in the forward-backward luminosity calorimeters for the events accepted by all other selection criteria. The hatched areas in (a) and (b) correspond to the contribution of $e^+\nu_e\ell^-\bar{\nu}_\ell$ final states. The arrows indicate the corresponding value of the applied cuts.

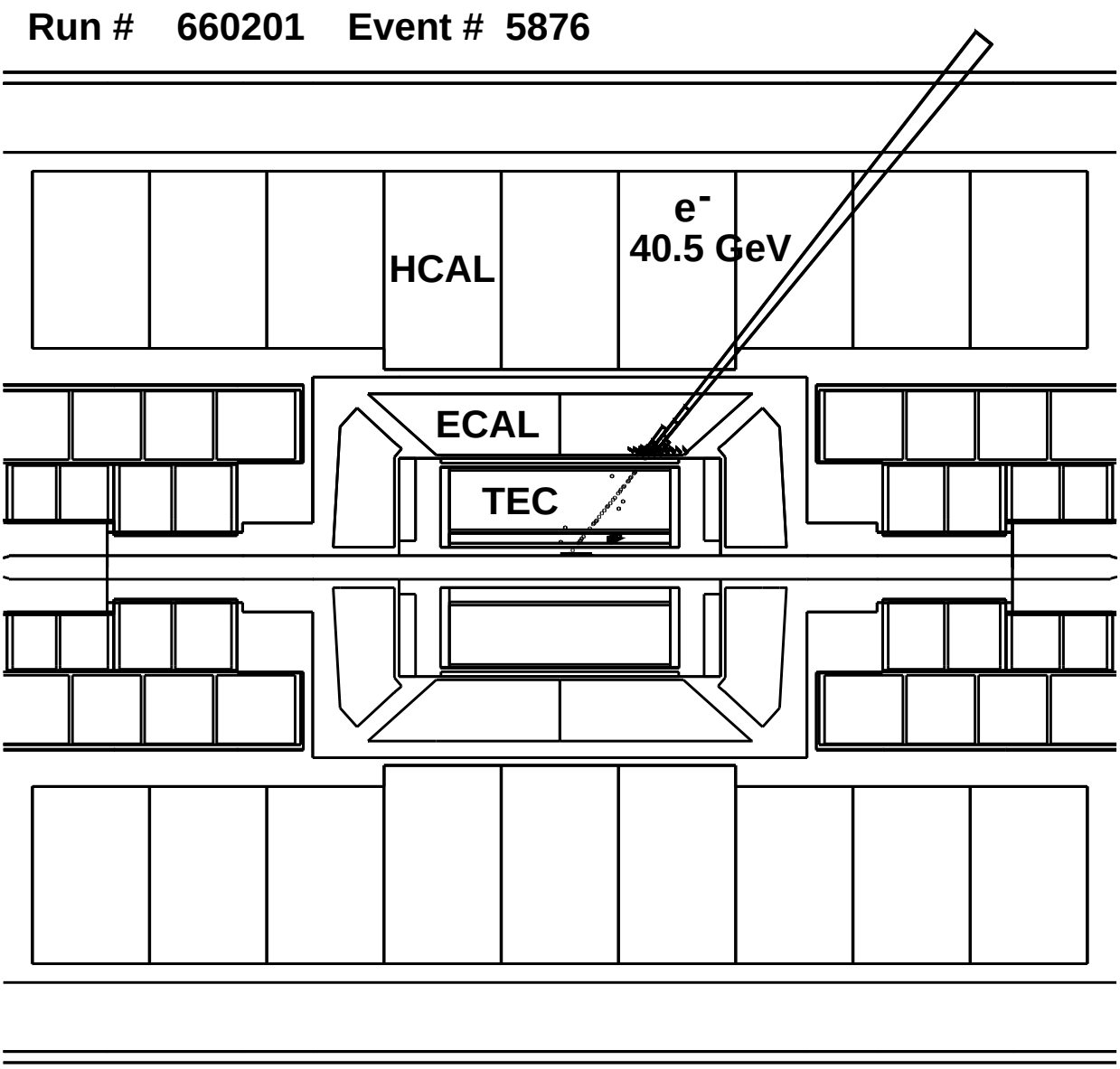

Figure 4: A $e^+e^- \rightarrow e^+\nu_e W^-$, $W^- \rightarrow e^-\bar{\nu}_e$ candidate event. In the upper hemisphere the 40.5 GeV electron is detected in the tracking chamber and in the electromagnetic calorimeter where the pulse heights represent the electron energy deposition . No significant energy deposition is observed in other subdetectors since the positron escapes in the beam pipe.

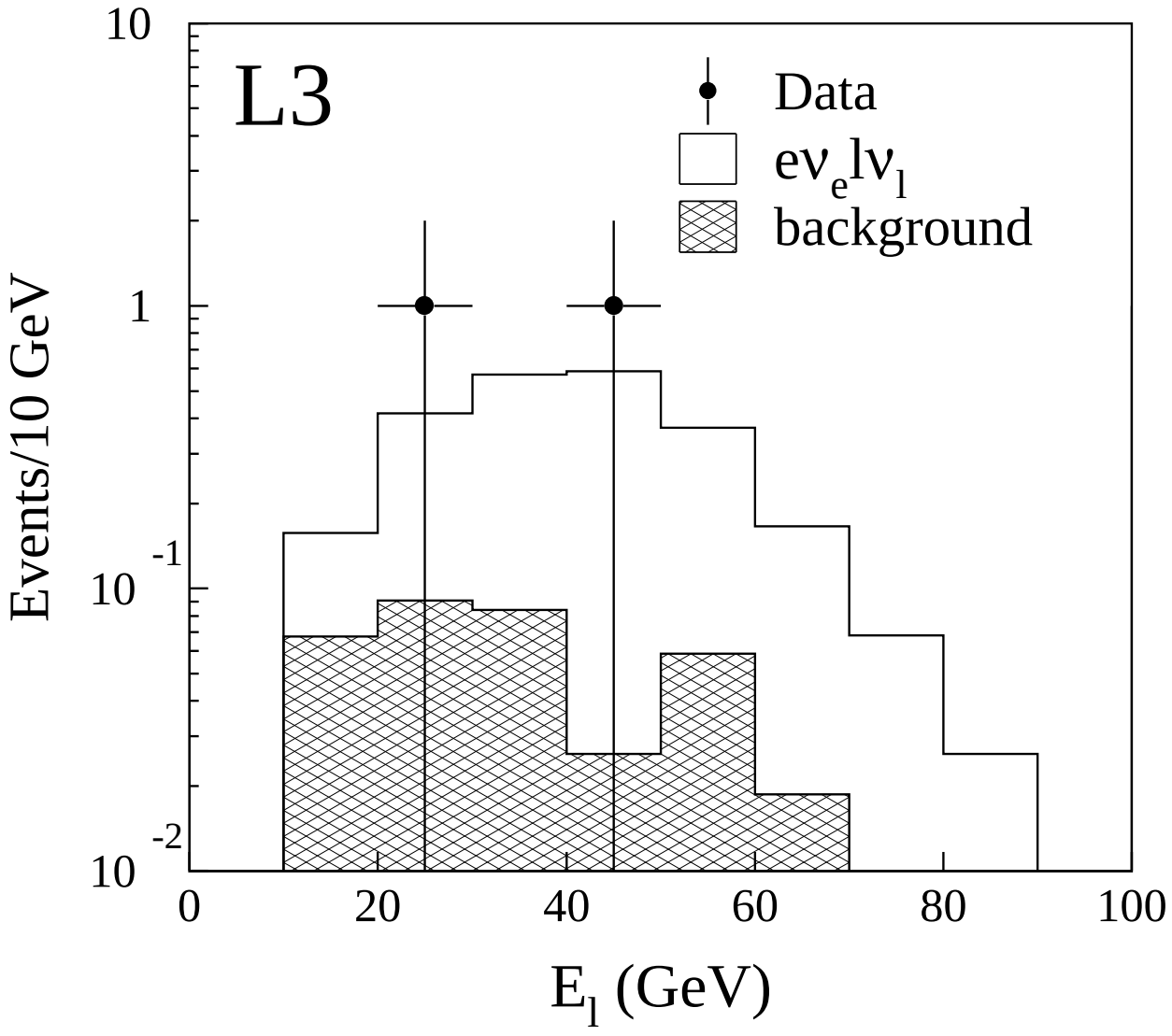

Figure 5: The energy spectrum of the selected leptonic candidates. The hatched histogram represents the background, the open histogram shows the fitted signal (2) from $e\nu_e\ell\nu_\ell$ final states.

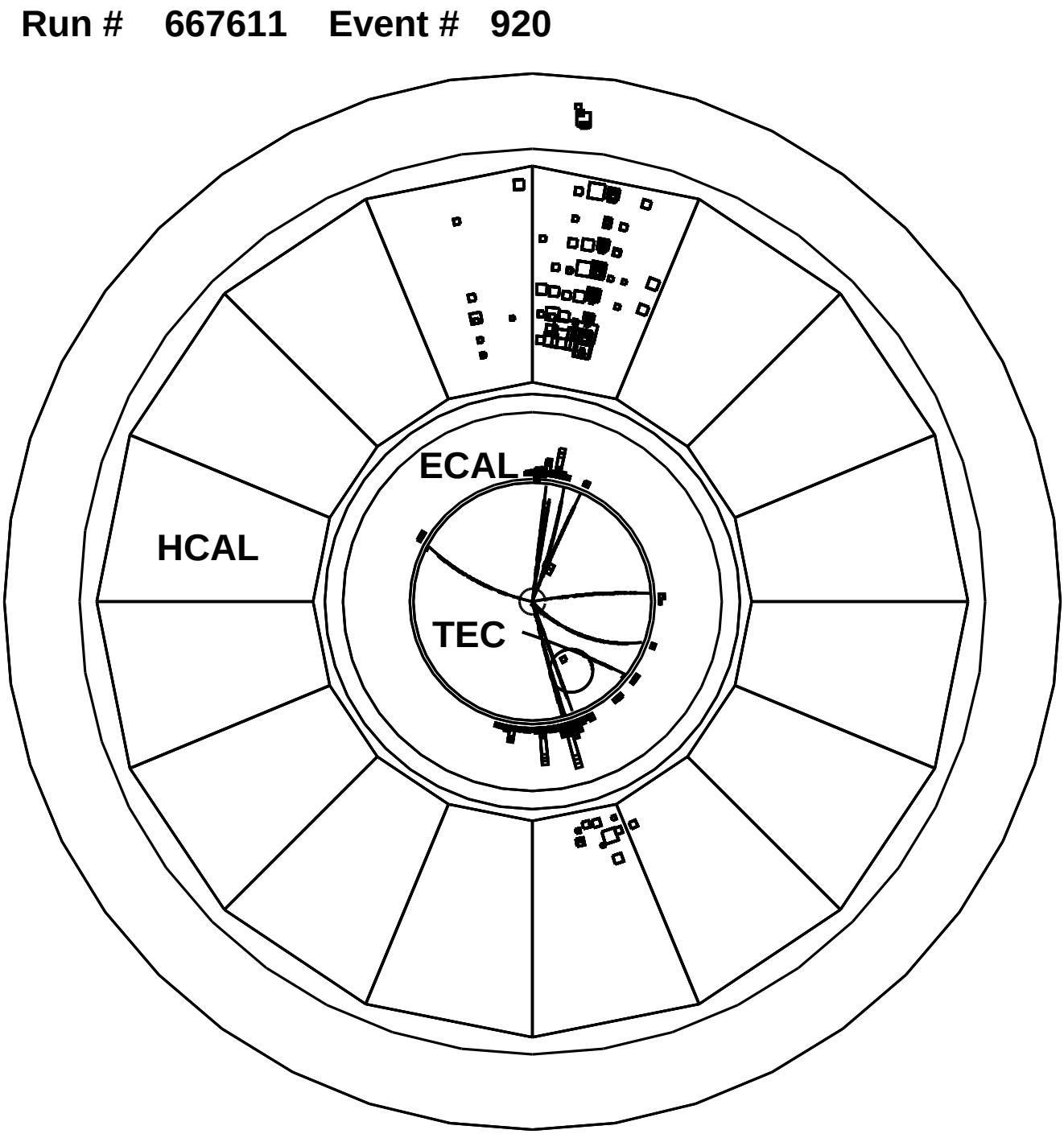

Figure 6: A candidate event for single W boson hadronic decay. The event consist of two acoplanar hadronic jets seen as groups of topologically connected tracks (TEC) and energy clusters (ECAL and HCAL). The pulse heights in the ECAL and size of squares in the HCAL are proportional to the energy depesition. The opening angle between the jets is 2.82 rad in the plane transverse to the beam direction. The jet-jet invariant mass is measured to be 91 GeV and the missing energy is 35 GeV in the transverse plane.

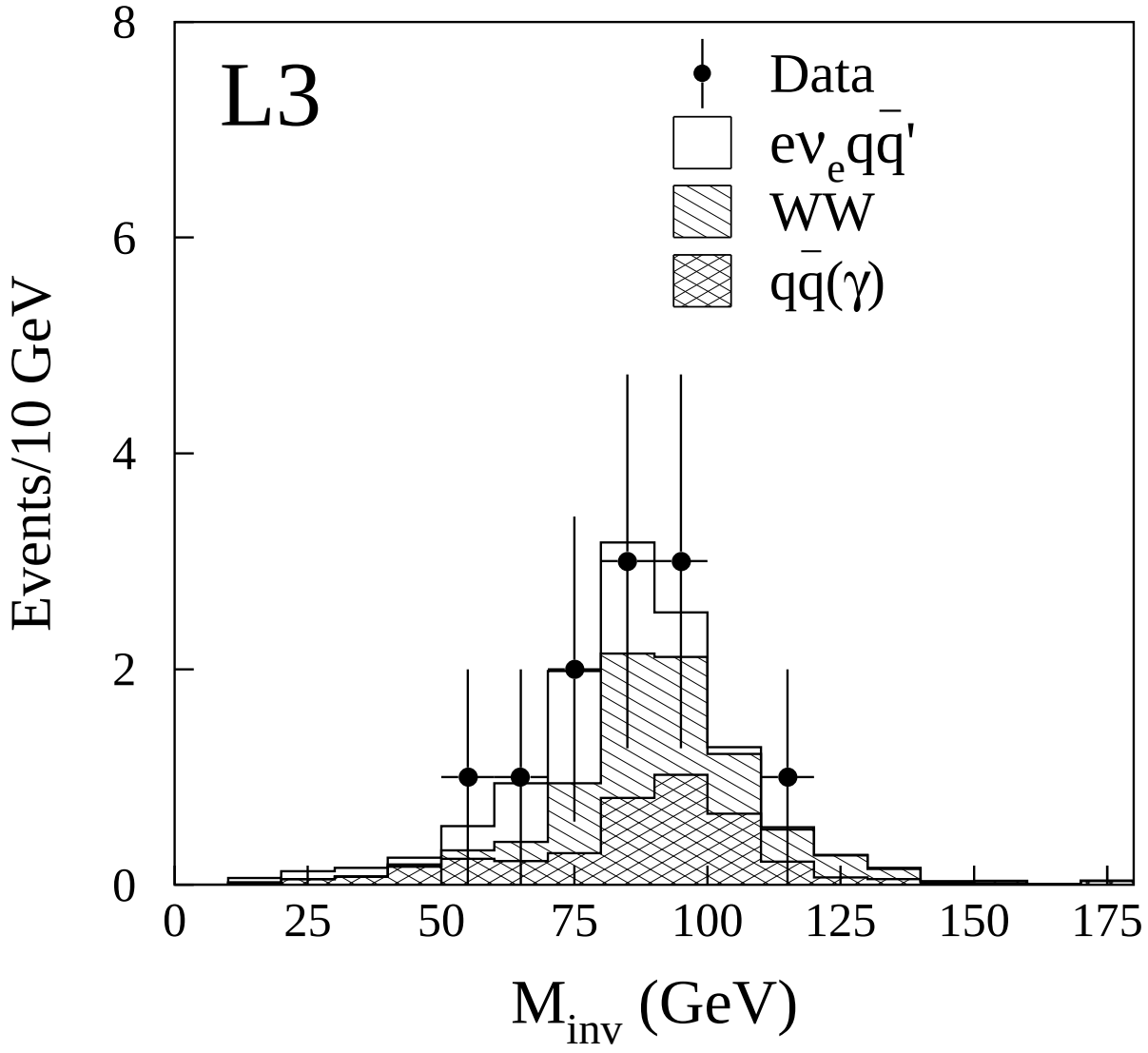

Figure 7: The jet-jet invariant mass spectrum, M_{inv} of the selected hadronic candidates for the combined data sample. The hatched histogram represents the background, the open histogram shows the fitted signal from $e^+\nu_e q\bar{q}'$ final states.

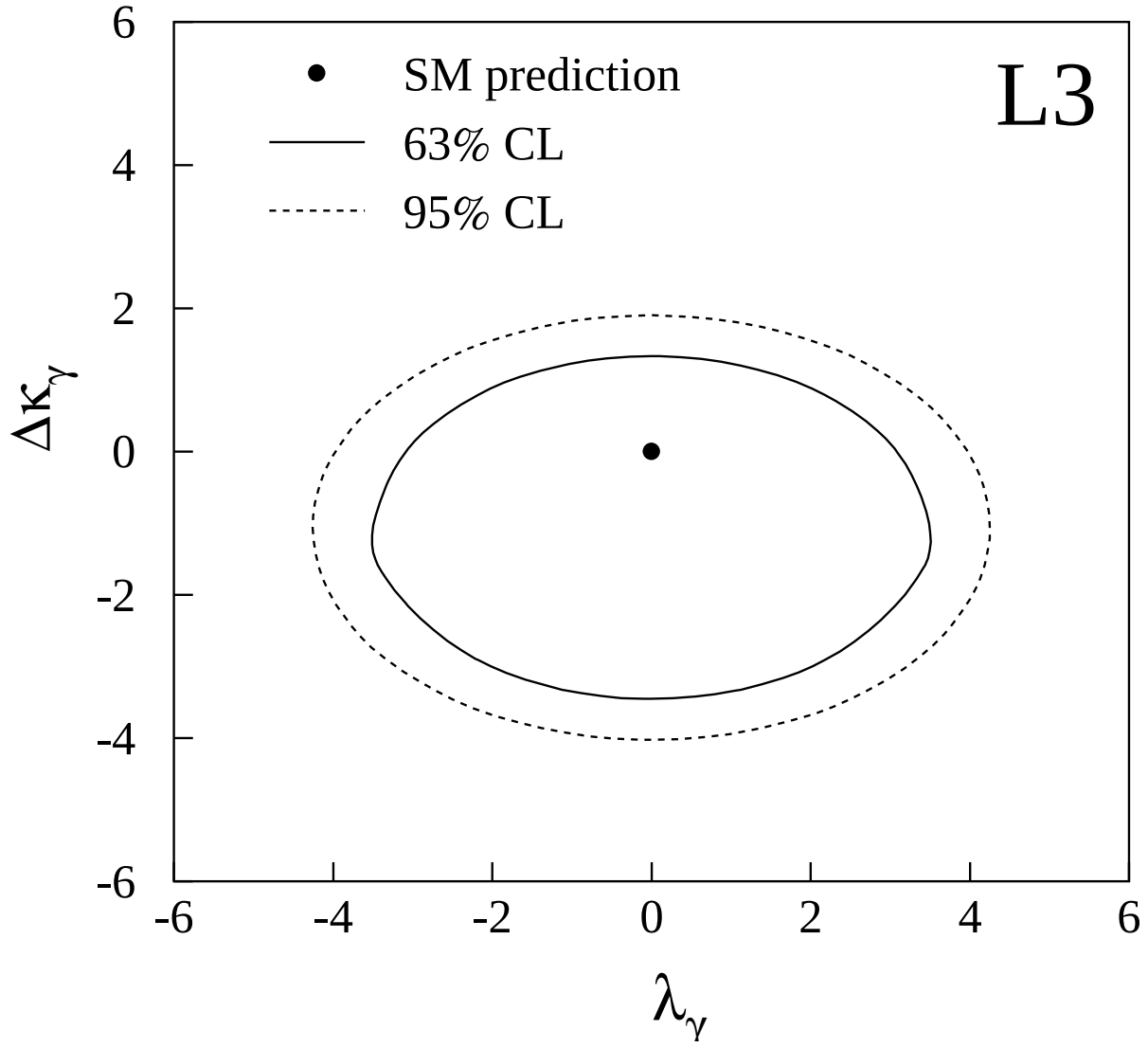

Figure 8: The contours corresponding to 63% and 95% confidence level exclusions in the $\Delta\kappa_\gamma - \lambda_\gamma$ plane.